6-2009

Synoptic-Scale Characteristics and Precursors of Cool-Season Precipitation Events at St. John's, Newfoundland, 1979-2005

Shawn M. Milrad
McGill University, milrads@erau.edu

Eyad H. Atallah
McGill University

John R. Gyakum
McGill University

Scholarly Commons Citation

Milrad, S. M., Atallah, E. H., & Gyakum, J. R. (2009). Synoptic-Scale Characteristics and Precursors of Cool-Season Precipitation Events at St. John's, Newfoundland, 1979-2005. *Weather and Forecasting, 24*(3). https://doi.org/10.1175/2008WAF2222167.1

Synoptic-Scale Characteristics and Precursors of Cool-Season Precipitation Events at St. John's, Newfoundland, 1979–2005

SHAWN M. MILRAD, EYAD H. ATALLAH, AND JOHN R. GYAKUM

Department of Atmospheric and Oceanic Sciences, McGill University, Montreal, Quebec, Canada

(Manuscript received 28 May 2008, in final form 14 November 2008)

ABSTRACT

The issue of quantitative precipitation forecasting continues to be a significant challenge in operational forecasting, particularly in regions susceptible to frequent and extreme precipitation events. St. John's, Newfoundland, Canada, is one location affected frequently by such events, particularly in the cool season (October–April). These events can include flooding rains, paralyzing snowfall, and damaging winds.

A precipitation climatology is developed at St. John's for 1979–2005, based on discrete precipitation events occurring over a time period of up to 48 h. Threshold amounts for three categories of precipitation events (extreme, moderate, and light) are statistically derived and utilized to categorize such events. Anomaly plots of sea level pressure (SLP), 500-hPa height, and precipitable water are produced for up to 3 days prior to the event. Results show that extreme events originate along the Gulf Coast of the United States, with the location of anomaly origin being farther to the north and west for consecutively weaker events, culminating in light events that originate from the upper Midwest of the United States and south-central Canada. In addition, upper-level precursor features are identified up to 3 days prior to the events and are mainly located over the west coast of North America.

Finally, results of a wind climatology produced for St. John's depict a gradual shift in the predominant wind direction (from easterly to southwesterly) of both the 925-hPa geostrophic wind and 10-m observed wind from extreme to light events, inclusively. In addition, extreme events are characterized by almost exclusively easterly winds.

1. Introduction

a. Motivation

One significant challenge in operational meteorology today is quantitative precipitation forecasting (QPF), particularly in regions of extreme precipitation events (Sisson and Gyakum 2004). As Doswell et al. (1996) point out, ''the task is not just to forecast the occurrence of an event, which is difficult enough by itself, but to anticipate the magnitude of the event....It is the amount of the precipitation that transforms an otherwise ordinary rainfall into an extraordinary, life-threatening situation.''

The accuracy of numerical model simulations of extratropical cyclones has progressed at an impressive rate over the past few decades. Both Bosart (1981) and Roebber and Bosart (1998) have concluded that while synoptic-scale mass-field forecasts (heights, sea level pressure, etc.) have improved dramatically over the past three or four decades, QPF progress has come at a much slower rate. Therefore, it is very important that efforts be made to aid the local forecaster in identifying significant synoptic-scale structures and precursors associated with precipitation events at a particular location. Lackmann and Gyakum (1996), Fischer (1997), Lackmann and Gyakum (1999), and Sisson and Gyakum (2004) accomplish this for the Northwest Territories; Montreal, Quebec, Canada; the Pacific Northwest of the United States; and Burlington, Vermont; respectively. Once particular patterns and/or precursors of different thresholds of precipitation events are identified, as was the case at the locations mentioned above, the local forecaster is able to use these benchmarks in addition to whatever forecast model(s) he or she is using.

Extreme precipitation events are prevalent and important in Atlantic Canada, where storms often cause hardship (Stewart et al. 1987), especially in the cool season

Corresponding author address: Shawn M. Milrad, Dept. of Atmospheric and Oceanic Sciences, McGill University, 805 Sherbrooke St. W., Montreal, QC H3A 2K6, Canada.
E-mail: shawn.milrad@mail.mcgill.ca

DOI: 10.1175/2008WAF2222167.1

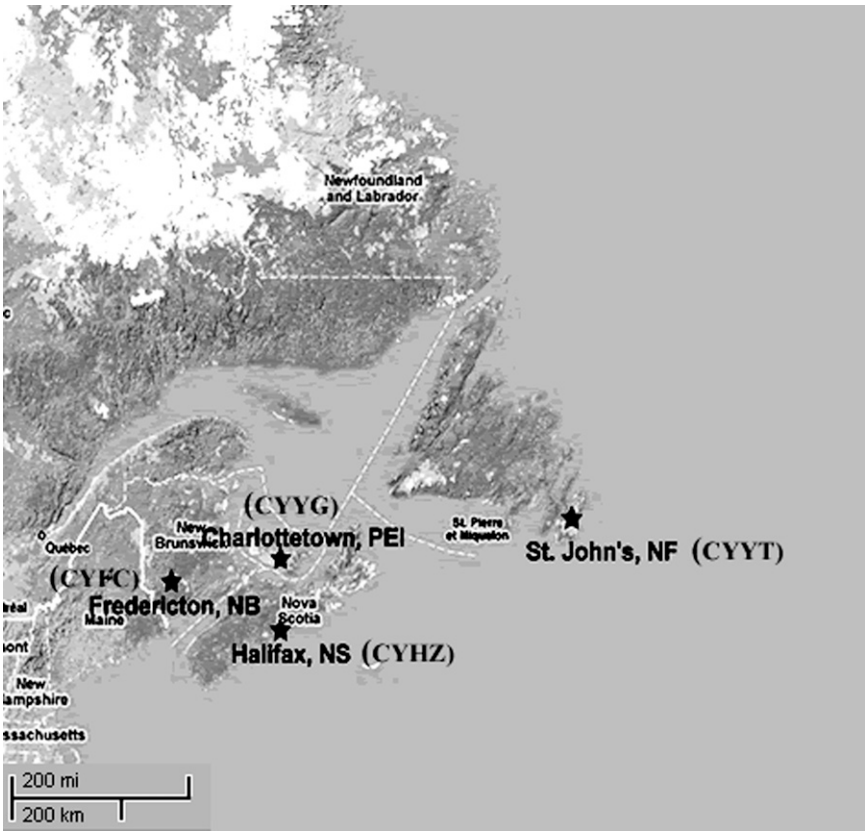

FIG. 1. The geography of Atlantic Canada, with the capital city of each province identified, and scale as shown.

(defined here as October–April). Atlantic Canada (Fig. 1), made up of the provinces of New Brunswick, Prince Edward Island, Nova Scotia, and Newfoundland and Labrador, is susceptible to major cool-season storms and resulting heavy precipitation (Stewart et al. 1987). This regional susceptibility is due primarily to the fact that Atlantic Canada is situated at the receiving end of several different storm tracks, in addition to being collocated at the confluence of the Gulf Stream and Labrador currents. If one assumes that each cyclone responsible for precipitation is associated with a midlevel (500 hPa) trough, as is usually the case, then the predominant climatological North American storm tracks during the months of October–April are depicted to end in Atlantic Canada (Fig. 2).

For this study, St. John's, Newfoundland, Canada, is chosen as the location of interest. In addition to being situated in a location commonly affected by several different storm tracks (Fig. 2), St. John's has the most precipitation events during our period of study (1979–2005) of all major stations in Atlantic Canada. This information is shown in Table 1, where from 1979 to 2005 St. John's recorded 1983 measurable (greater than or equal to 0.2 mm or 0.01 in.) cool-season precipitation events, 112 more than any other capital city in Atlantic Canada. In addition, St. John's has the highest average amount of precipitation (Table 2) among the four capital cities in Atlantic Canada (the other capitals being Fredericton, New Brunswick; Charlottetown, Prince Edward Island; and Halifax, Nova Scotia).

b. Objectives and methodology

Given that St. John's has such a preponderance of precipitation, our objective is to identify synoptic-scale characteristics and precursors to cool-season precipitation events of varying intensities. Furthermore, it will be determined whether there are dynamical precursors that are particularly unique to the more extreme events. As such, the remainder of this paper is organized as follows:

1) A cool-season (October–April) precipitation climatology is established at St. John's (CYYT) from 1979 to 2005, and statistics (e.g., mean, median, standard deviation) associated with this climatology are calculated.

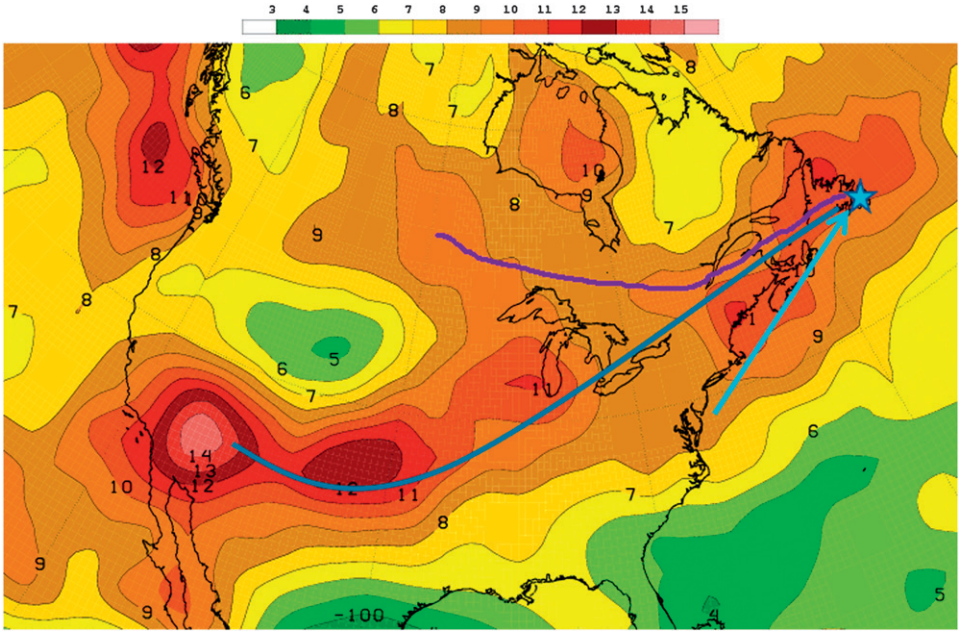

FIG. 2. October–April 30-yr (1971–2000) climatological frequency of 500-hPa absolute vorticity centers, calculated by counting the number of absolute vorticity maxima in the region shown; this roughly depicts the mean North American storm tracks and their importance to Atlantic Canada. The units are numbers of events per 5° × 5° area (approximately 500 km^2).

2) Using our computed climatological statistics, we establish three categorical thresholds of precipitation events: extreme, moderate, and light.
3) Given the aforementioned categorical thresholds of precipitation, we identify synoptic-scale characteristics of these precipitation event groups. This is done primarily by compositing a representative subset of events for each precipitation threshold. It will be shown that differences exist among the different precipitation thresholds in terms of large-scale structural anomalies and precursors up to 72 h prior to the precipitation event. Both dynamical and moisture fields will be examined, including sea level pressure (SLP), 500-hPa height, and precipitable water.
4) An analysis of the observed surface and near-surface geostrophic wind distributions at St. John's is performed to reinforce conclusions depicted in the dynamical and moisture composite fields.

2. Data

This study utilizes 6-hourly precipitation data for St. John's, courtesy of the Environment Canada 6-h corrected precipitation database (Environment Canada Atlantic Climate Centre 2007, personal communication). The corrected precipitation data are based on work done by Mekis and Hogg (1999), whereby the data have been adjusted to accurately reflect precipitation gauge changes, wind conditions, and changes in station location. It is also of note that all precipitation data in this study are observed in liquid equivalent form (i.e., no data were acquired using ruler methods), thus in theory limiting the errors one might expect at a station such as St. John's, where frozen precipitation is commonplace. The National Centers for Environmental Prediction–National Center for Atmospheric Research (NCEP–NCAR) global reanalysis dataset, with a horizontal resolution of 2.5° × 2.5° (Kalnay et al. 1996), is used as the dataset of choice for all synoptic-scale composite and anomaly plots. The overwhelming majority of the calculations and analyses in this study are performed and displayed using the General Meteorological Package, version 5.7.4 [GEMPAK, updated from the original

TABLE 1. The number of cool-season (October–April) measurable precipitation events at four selected station in Atlantic Canada.

Location	No. of cool-season measurable precipitation events (1979–2005)
Fredericton, NB (CYFC)	1531
Charlottetown, PEI (CYYG)	1871
Halifax, NS (CYHZ)	1742
St. John's, NF (CYYT)	1983

TABLE 2. Mean monthly precipitation amounts for the four capital cities in Atlantic Canada during the cool season (October–April).

	Fredericton (mm)	Charlottetown (mm)	Halifax (mm)	St. John's (mm)
Oct	97.7	108.6	128.7	161.9
Nov	103.2	110.8	146	144
Dec	107.8	123.1	154.8	148.8
Jan	109.6	106.4	149.2	150
Feb	79.2	85.5	114.4	125.2
Mar	102.7	91.8	134.5	130.8
Apr	87.4	87.8	118.3	121.8
Tot	687.6	714	945.9	982.5

package devised by Koch et al. (1983)], a data manipulation and visualization software package commonly used in synoptic analyses. In section 5 (wind climatology and analysis), the wind rose plots are created using WRPLOT view, a program developed by Lakes Environmental, Inc., (available online http://www.weblakes.com/lakewrpl.html). Actual surface station data are used for the 10-m observed wind values, and NCEP–NCAR global reanalysis data are used for the 925-hPa geostrophic wind values.

3. Precipitation climatology methodology

As previously detailed and as shown in Table 2, the average total amount of liquid equivalent precipitation at St. John's during the cool season is 982.5 mm. The highest monthly average amount is 161.9 mm during October, when (a) convection may still be present with strong cold frontal passages and (b) a number of tropical or recently transitioned extratropical cyclones have been known to influence the region (Hart and Evans 2001). November, December, and January have similar amounts of average precipitation, while there is a stark dropoff in precipitation during February. While not crucial to this particular study, it is speculated here that this dropoff may be due in part to several factors, including more sea ice in the region (and therefore less surface moisture flux for a given storm to work with). This considered, however, St. John's receives more precipitation on average for every month in the defined cool season than does any of the other capital cities in Atlantic Canada, with the exceptions of Halifax in November, December, and March.

To compile a database of precipitation events for this study, we take the 6-hourly precipitation data provided and locate events that range anywhere from one precipitation recording period (6 h) to eight recording periods (48 h). This is done to keep a reasonable synoptic time scale in mind when compiling a list of events. Additionally, to ensure separation of precipitation events, there must be no fewer than two recording periods (12 h) of zero precipitation. Finally, an event must consist of at least 0.2 mm of precipitation. Given the parameters above, 1983 measureable precipitation events were recorded in the cool season from 1979 to 2005 (Table 1). As previously discussed, this is a larger number than that of any other capital city in Atlantic Canada during the same time period.

The next step in the process is to statistically analyze and separate the 1983 measureable precipitation events recorded at St. John's from 1979 to 2005. Here, we utilize a normal distribution, following the methodology of the work done on warm-season precipitation events at Burlington, Vermont (Atallah et al. 2005). Accordingly, the mean precipitation amount (9.80 mm) and standard deviation (11.99 mm) are calculated. It is evident from the large value of the standard deviation that precipitation event amounts at St. John's are quite variable and can range anywhere from the minimum of 0.2 mm to a maximum of 82.2 mm. Once the mean and standard deviation have been calculated, the next step is to identify bins, or categorical thresholds, of precipitation amounts. This is done in a fashion similar to Atallah et al. (2005), whereby events with amounts of the mean plus 2 standard deviations or more ($>$33.78 mm) are labeled extreme, the mean plus 0.5–1 standard deviation (15.81–21.79 mm) are moderate events, and the mean $\pm$0.5 standard deviation (3.81–15.8 mm) are light events. As a result, we find 106 extreme events, 160 moderate events, and 681 light events. It is evident (Fig. 3) that the number of light events (681) is more than double the value of the other categories combined, reinforcing the conclusion put forth by Sisson and Gyakum (2004) that light events tend to dominate the climatology at a given station. Finally, while the authors acknowledge the fact that using a normal distribution in this study is unorthodox, it is a primary objective of this study to create categories of precipitation events that are well separated from each other. The authors believe that this objective has been accomplished with the creation of the extreme, moderate, and light categories, whereby the median amount in each category falls in the 97th, 82nd, or 60th percentile, respectively (Fig. 3). It is true that the majority of cases (Fig. 3) are events with very small amounts of precipitation (5 mm or less), but these are generally cases that are not of concern in terms of forecasting. Using our methodology, we identify three distinctly separate, but important, classes of precipitation events. This classification can be used to conduct a synoptic analysis.

To deal with an equal number of cases in each category, we follow the methodology of Sisson and Gyakum

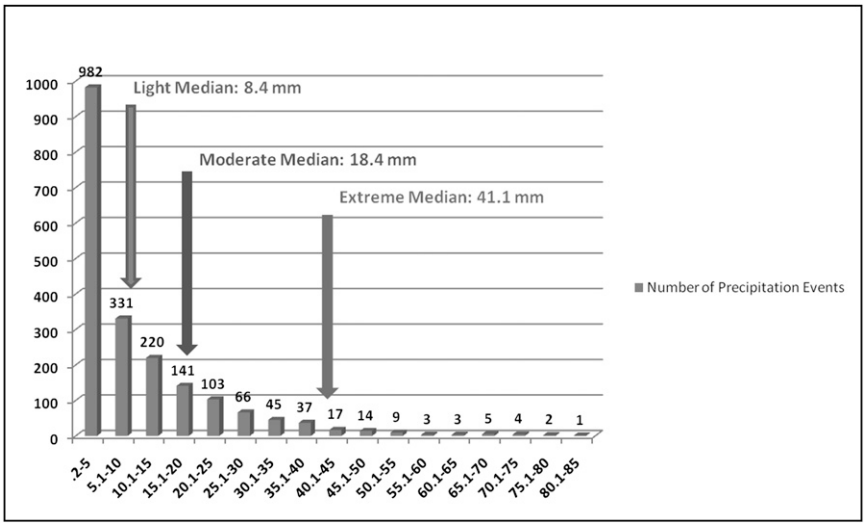

FIG. 3. The precipitation event distribution histogram, depicting bins every 5 mm, and with the median of each precipitation category indicated.

(2004) and select 50 events from each category to be used in the composite synoptic analyses in the following chapter. To accomplish this, the median for each category (as computed using the mean and standard deviation methodology described above) of precipitation events is calculated; this value is 41.1 mm for extreme events, 18.4 mm for moderate events, and 8.4 mm for light events. Twenty-five events above and below the median for each category are taken as the group of 50 events to be utilized for synoptic compositing. The ranges of the 50 precipitation events in each category are as follows: 38.2–48.6 mm for the extreme events, 17.5–19.3 mm for the moderate events, and 8–8.8 mm for the light events.

4. Composite results

a. Methodology

As Sisson and Gyakum (2004) point out, the reason for completing and displaying composite analyses is to ''identify key synoptic-scale circulation features, and their climatological anomalies, associated with each of the intensities of precipitation.'' Moreover, examining circulation anomalies in addition to the full composite fields allows the depiction of the significance of a particular feature with respect to a monthly weighted 30-yr (1971–2000) climatology derived from the NCEP–NCAR global reanalysis dataset. In this study, composite and anomaly plots of selected atmospheric mass fields are displayed every 12 h (these fields have been examined every 6 h but, due to space concerns, are shown every 12) from $t = -48$ h to $t = +12$ h ($t = -72$ to $+24$ h for the 500-hPa height anomaly plots; this is done specifically because statistically significant 500-hPa height anomalies are observed as early as $t = -72$ h), where $t = 0$ h is the time of onset of the heaviest precipitation period. First, sea level pressure anomalies are examined, followed by 500-hPa height and precipitable water. In the case of the 500-hPa height composites, a larger view is chosen for display to emphasize the importance of upstream anomalies. It should be noted that the precursor anomalies depicted in the 500-hPa height composites, while valid, should not be fully used in an operational sense until a check of null events has been completed. This is something that will be explored in future work. Finally, it is unclear exactly how much smearing there is involved with the composite process; however, while some smearing is to be expected in all composites, frequency maps of 500-hPa vorticity and 850-hPa height (similar to Fig. 2 but not shown for sake of brevity) depict storm tracks that are very similar to the composite mean tracks observed for all three precipitation intensity groups (extreme, moderate, and light).

b. Sea level pressure (SLP)

1) EXTREME PRECIPITATION CASES

In the extreme precipitation cases (Fig. 4), the first sign of a statistically significant (at the 99% confidence level) negative SLP anomaly occurs at $t = -48$ h (Fig. 4a) and is centered over the southeastern United States. As the anomaly tracks northeastward over time, it grows in amplitude before it reaches a maximum of -18 hPa at $t = 0$ h (Fig. 4e) near St. John's. It is also worth noting that a significant positive SLP anomaly develops downstream of

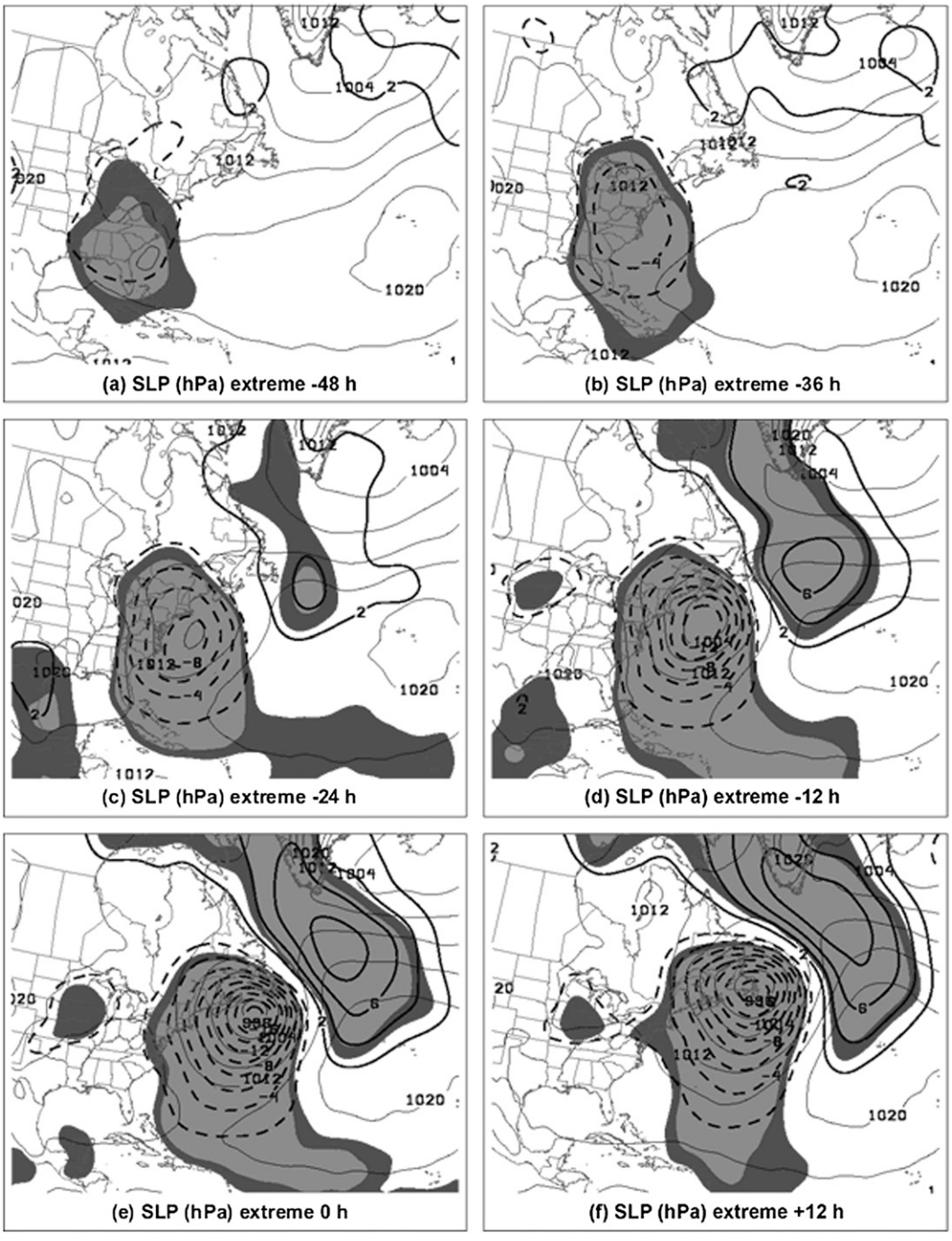

FIG. 4. SLP anomalies every 2 hPa, heavy dashed for negative values and heavy solid for positive values, with respect to climatology, for the extreme cases at (a) −48, (b) −36, (c) −24, (d) −12, (e) 0, and (f) +12 h. Light solid contours represent the full composite SLP field, every 4 hPa. Shading represents the statistical significance of the anomalies at the 95% (lighter shading) and 99% (darker shading) confidence levels, according to the Student's *t* test.

the negative anomaly, beginning at $t = -24$ h (Fig. 4c) and grows in amplitude until it reaches a maximum intensity (highest closed contour) of +8 hPa at $t = 0$ h (Fig. 4e).

In terms of the strengthening over time of the downstream positive SLP anomaly, it is important to recognize that two processes are in play here. First, a stronger negative SLP anomaly would lead to strong warm-air

advection decreasing with height, which would act to raise heights in the upper levels of the atmosphere, that is, build an upper-level ridge just downstream of the surface SLP negative anomaly (Figs. 7f and 7g). This in turn would help to strengthen the surface positive SLP anomaly downstream of the upper-level ridge (Figs. 4c–f). Second, as extreme precipitation falls in association with the negative anomaly, latent heat release in the lower levels of the atmosphere acts to diabatically enhance the upper-level ridge located just downstream of the surface cyclone around $t = 0$ h (Figs. 7f and 7g). Consequently, the suggestion is that the diabatic enhancement of the upper-level ridge could also partially be responsible for the building of stronger surface high pressure downstream, as is evident in the time evolution of the extreme SLP composite (Figs. 4c–f). Nevertheless, it is important to recognize that while the warm-air advection and diabatic enhancement processes have the same effect, it is likely that both are at work here.

2) MODERATE PRECIPITATION CASES

A statistically significant negative SLP anomaly in the moderate composite is evident as early as $t = -48$ h (Fig. 5a) over the Ohio River valley. The initial location of the negative anomaly is farther north and west than in the extreme (Fig. 4a) composite. In addition, the negative anomaly proceeds on a more land-based track compared with the extreme composite. It is also of note that at $t = +12$ h (Fig. 4f), the statistically significant downstream positive SLP anomaly is less intense (by 2 hPa) and less broad than in the extreme composite. This is a suggestion that either or both of the indirect processes described above (warm-air advection and the latent heating feedback mechanism) might have less of an impact in the moderate cases than in the extreme cases, as one would expect with both a weaker negative SLP anomaly and lesser amounts of precipitation.

3) LIGHT PRECIPITATION CASES

As in the extreme precipitation composites, a coherent statistically significant negative SLP anomaly is observed at $t = -48$ h (Fig. 6a). However, this negative anomaly is located over the upper Midwest region of the United States, far north and west of the initial anomalies in the extreme (Fig. 4a) and moderate (Fig. 5a) composites. Also unique to the light composite is the pure zonal track of the negative anomaly toward St. John's (Figs. 6a–e). Moreover, the negative anomaly reaches a maximum intensity of only -8 hPa at $t = 0$ h (Fig. 6e), which is significantly weaker than the other precipitation intensities. Finally, a weak downstream positive anomaly appears at $t = -12$ h (Fig. 6d), but only reaches a maximum intensity of 4 hPa at $t = 0$ h (Fig. 6e) and $t = +12$ h (Fig. 6f), weaker than the positive anomalies in the other precipitation intensity composites. In the light composite, the cyclone responsible for the precipitation at St. John's resembles an Alberta clipper that forms in the lee cyclogenesis region of the Canadian Rockies.

c. 500-hPa height

1) EXTREME PRECIPITATION CASES

In the extreme precipitation composite, a statistically significant (at the 95% confidence level) positive anomaly is located over the Pacific Northwest region of the United States at $t = -72$ h (Fig. 7a). This anomaly grows in both areal extent and intensity by $t = -36$ h (Fig. 7d), at which time the first significant negative anomaly appears just east of the Mississippi River. Twelve hours later, at $t = -24$ h (Fig. 7e), a significant downstream ridge is located right over St. John's. As time proceeds, both the negative anomaly and downstream positive anomaly grow in amplitude, while the upstream ridge weakens accordingly. The suggestion here is that the precursor ridge over the Pacific Northwest leads to downstream development of the negative anomaly over the Ohio River valley, which in turn leads to the downstream ridge over Atlantic Canada. Similar features were noted by Lackmann and Gyakum (1996) in their study of precursor anomalies in the Northwest Territories of Canada. In their study, as well as in this one, the decay of the upstream ridge at the same time at which both the negative anomaly and the downstream ridge amplify is consistent with the downstream propagation of Rossby wave energy with the group velocity (Lackmann and Gyakum 1996).

This assertion of downstream development is supported with a time–longitude plot of the meridional (v) component of the wind at 500 hPa (Fig. 8). Figure 8 shows that in the extreme composite, a weak positive anomaly is seen around 130°W beginning between $t = -72$ and -60 h, in association with the precursor positive height anomaly (Fig. 7a). This weak positive wind anomaly gives way to a stronger downstream (100°W) negative anomaly beginning at $t = -48$ h (and peaking at $t = -24$ h), in association with the negative height anomaly seen over the southeastern United States (Fig. 9). In turn, a downstream positive and a second negative anomaly form at $t = -24$ h (70°W) and $t = 0$ h (30°W), respectively. It is implied here (Fig. 8) that the downstream propagation of Rossby wave energy is evident in the extreme composite, as each 500-hPa meridional wind anomaly maximum lags the previous anomaly maximum in time.

It is also important to note that at $t = 0$ h (Fig. 7g), the negative anomaly associated with the surface cyclone

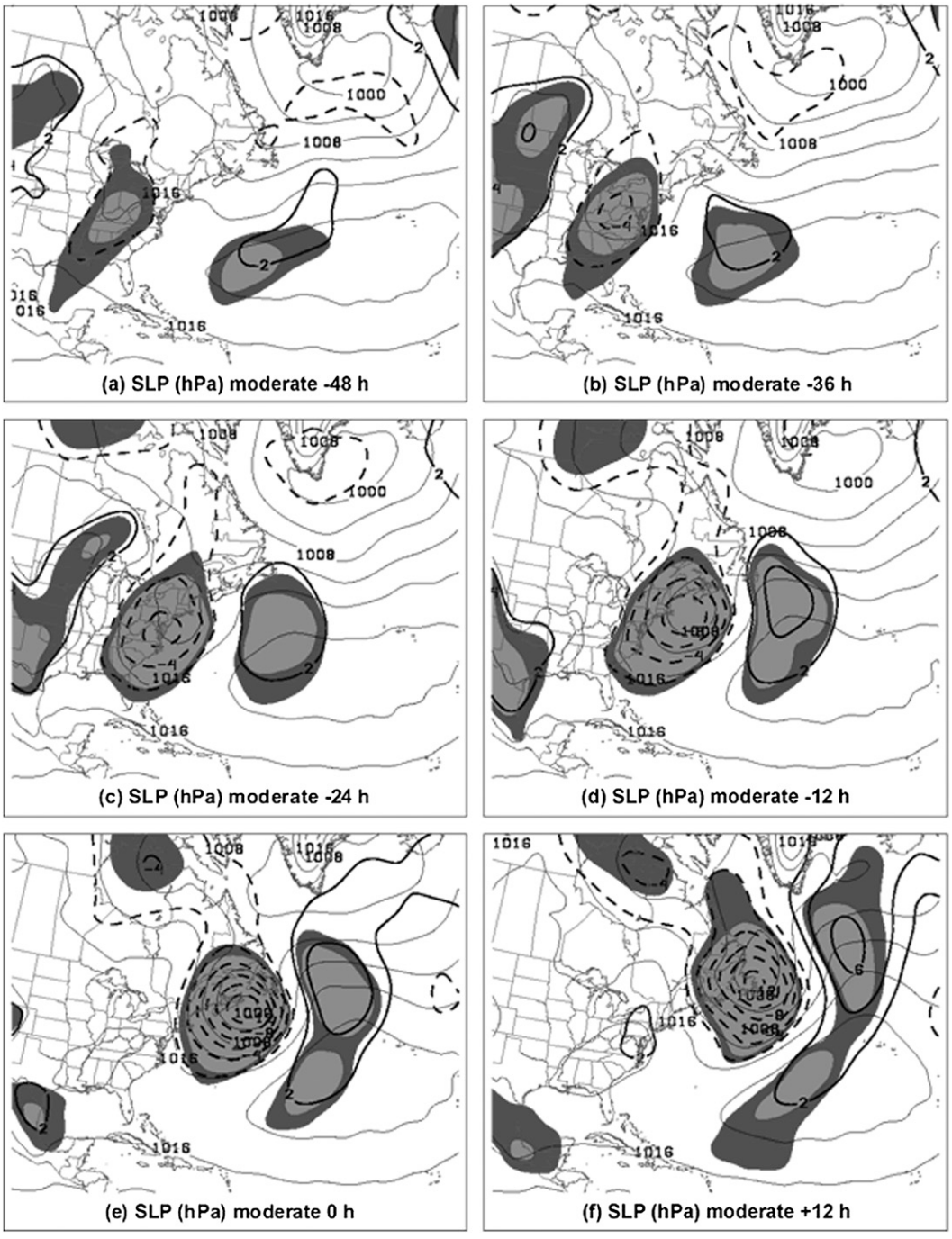

FIG. 5. As in Fig. 4, but for the moderate cases.

affecting St. John's has reached a maximum of −120 m and the downstream positive anomaly has reached a maximum of +120 m, while the upstream ridge essentially disappears. The increase in amplitude of the negative anomaly associated with the surface cyclone suggests a positive increase in cyclonic vorticity advection at 500 hPa, which in turn would act to strengthen the surface cyclone.

2) MODERATE PRECIPITATION CASES

A precursor positive anomaly is depicted at $t = -72$ h (Fig. 9a); unlike in the extreme cases, however, the positive anomaly is located much farther to the north near the Gulf of Alaska. As time progresses, the positive anomaly extends southward into the Pacific Northwest region of the United States, and is of similar strength to

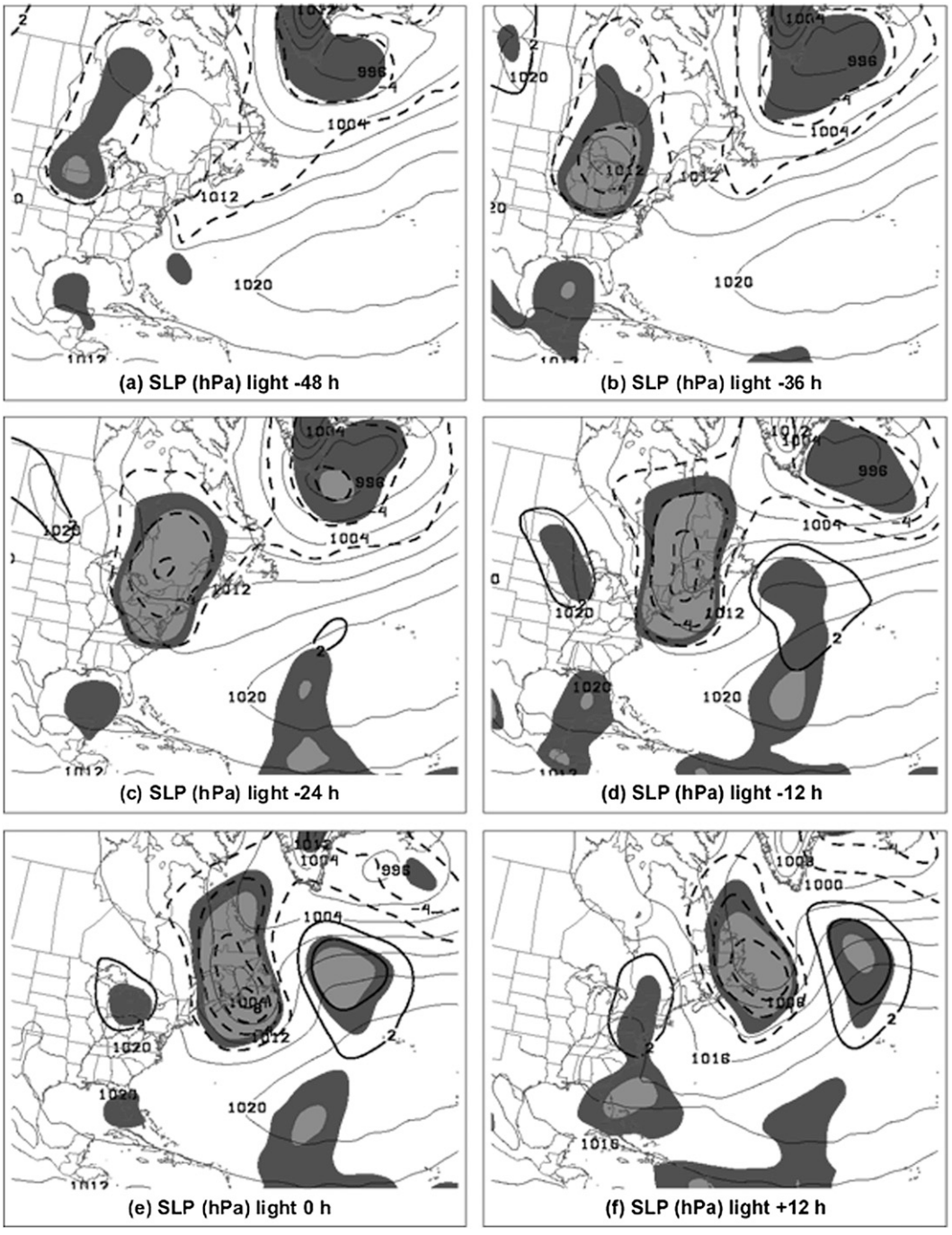

FIG. 6. As in Fig. 4, but for the light cases.

the corresponding positive anomaly in the extreme composite at $t = -36$ h (Fig. 9d). Unlike in the extreme cases, however, the upstream positive anomaly does not shrink in areal extent or propagate eastward as time progresses.

The moderate cases are also different from any other precipitation intensity category because of the large areal extent of the negative anomaly over the eastern third of North America. This suggests that the track variability of the negative anomaly (trough) is largest in the moderate cases. While track variability is not examined explicitly in this paper, this will be a primary focus of future studies. In addition, the weaker downstream positive anomaly (+90 m at $t = 0$ h; Fig. 9g) suggests four possible conclusions: (a) the weaker negative SLP anomaly (Fig. 5) produces less low-level

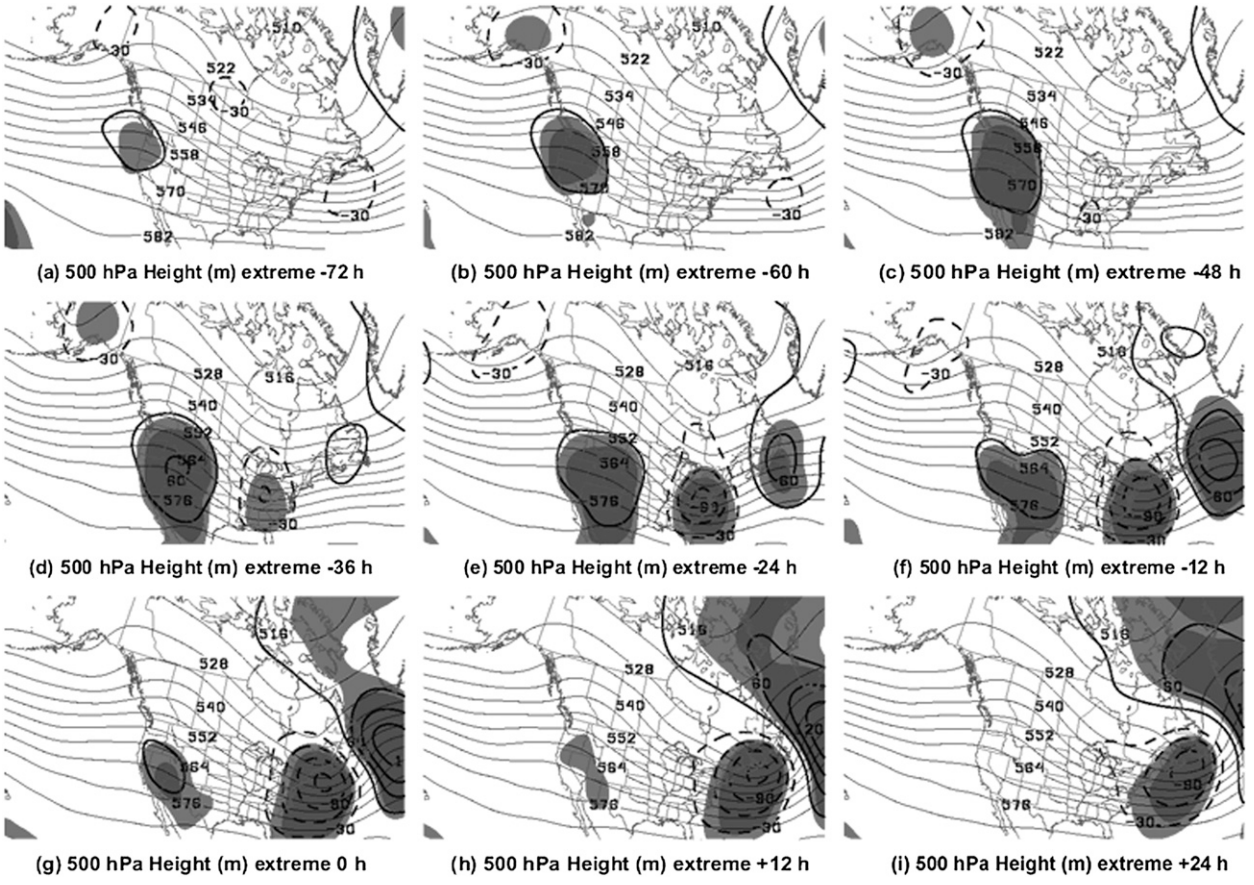

FIG. 7. The 500-hPa height anomalies every 3 dam, heavy dashed for negative values and heavy solid for positive values, with respect to climatology for the composite of the extreme cases at (a) −72, (b) −60, (c) −48, (d) −36, (e) −24, (f) −12, (g) 0, (h) +12, and (i) +24 h. Light solid contours represent the full composite 500-hPa field, every 6 dam. Shading represents the statistical significance of the anomalies at the 95% (lighter shading) and 99% (darker shading) confidence levels, according to the Student's *t* test.

warm-air advection, leading to a weaker upper-level ridge (Fig. 9); (b) the reduced overall precipitation associated with the surface cyclone produces less latent heat release and thus less downstream ridge intensification; (c) the lack of weakening of the upstream positive anomaly is suggestive of the lack of downstream positive anomaly amplification; and (d) a combination of possibilities a–c above.

Finally, in terms of downstream development, a time–longitude plot for the moderate cases (Fig. 10) shows that while the initial weak positive 500-hPa meridional wind component anomaly is farther to the west at $t = -72$ and -60 h than in the extreme (Fig. 8) composite, Fig. 10 does display a surprisingly coherent downstream development signal. The first negative meridional wind anomaly forms near 100°W at $t = -36$ h; although this anomaly is weaker than the negative anomaly seen in the extreme composite (Fig. 8), it does seem to excite a downstream positive (70°W) and second negative anomaly (40°W) at $t = -24$ and 0 h, respectively. This structure is very similar to the downstream development seen in the extreme cases (Fig. 8) and corresponds with the associated 500-hPa height anomalies observed for the moderate cases (Fig. 9).

3) LIGHT PRECIPITATION CASES

As in the SLP composites, the light precipitation cases depict synoptic structures that are entirely different from the other precipitation intensities. In the light precipitation cases, a positive anomaly is apparent over western British Columbia at $t = -72$ h (Fig. 11a). However, unlike in the other three precipitation intensity composites, this precursor positive anomaly has reached its maximum strength at $t = -72$ h (Fig. 11a) and actually proceeds to retrogress northward into Alaska, as is evident by $t = -36$ h (Fig. 11d). At this time, a statistically significant negative height anomaly becomes visible over the upper Midwest region of the United States and western Ontario. This formation location of the negative anomaly is farther to the north than in any

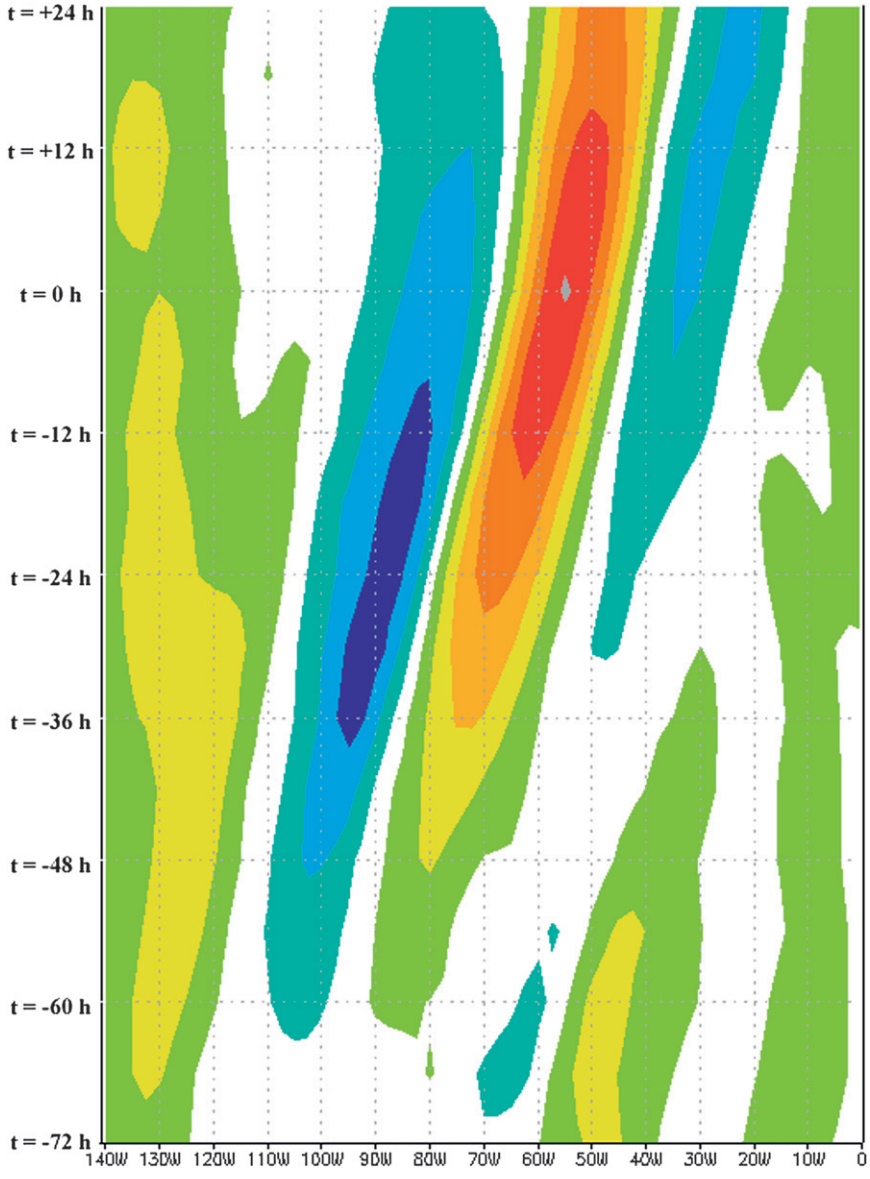

FIG. 8. Time–longitude plot of the 500-hPa meridional (v) component of the wind anomalies relative to climatology at 40°N (every 3 m s^{-1}, shaded warm colors for positive and cool colors for negative) for the extreme cases from $t = -72$ to $+24$ h.

of the other precipitation intensities, supporting the observation from the light SLP composite that light events are primarily driven by quick-moving Alberta clipper systems that do not appear to have access to Gulf of Mexico moisture. In addition, a downstream positive anomaly is nearly nonexistent, until a weak ridge appears at $t = 0$ h (Fig. 11g), east of St. John's. It is likely not coincidental that this occurs just as the negative anomaly reaches the Atlantic Ocean, finally encountering a significant moisture source. While the negative anomaly does reach an intensity, -90 m, at $t = +12$ h (Fig. 11h), that is similar to that of the negative anomalies moderate composite (Fig. 9h), the upstream positive anomaly is almost entirely nonexistent from early in the progression, and the downstream ridge is very weak, suggesting that downstream development plays a significantly reduced role here than it does in the other precipitation intensity composites. A time–longitude plot of the meridional wind component (Fig. 12) shows a weaker signal of downstream development than that seen in the extreme (Fig. 8) and moderate (Fig. 10) composites. In addition, the positive and negative 500-hPa meridional wind anomalies are observed (Fig. 12) at later initial times, in association with the height anomalies

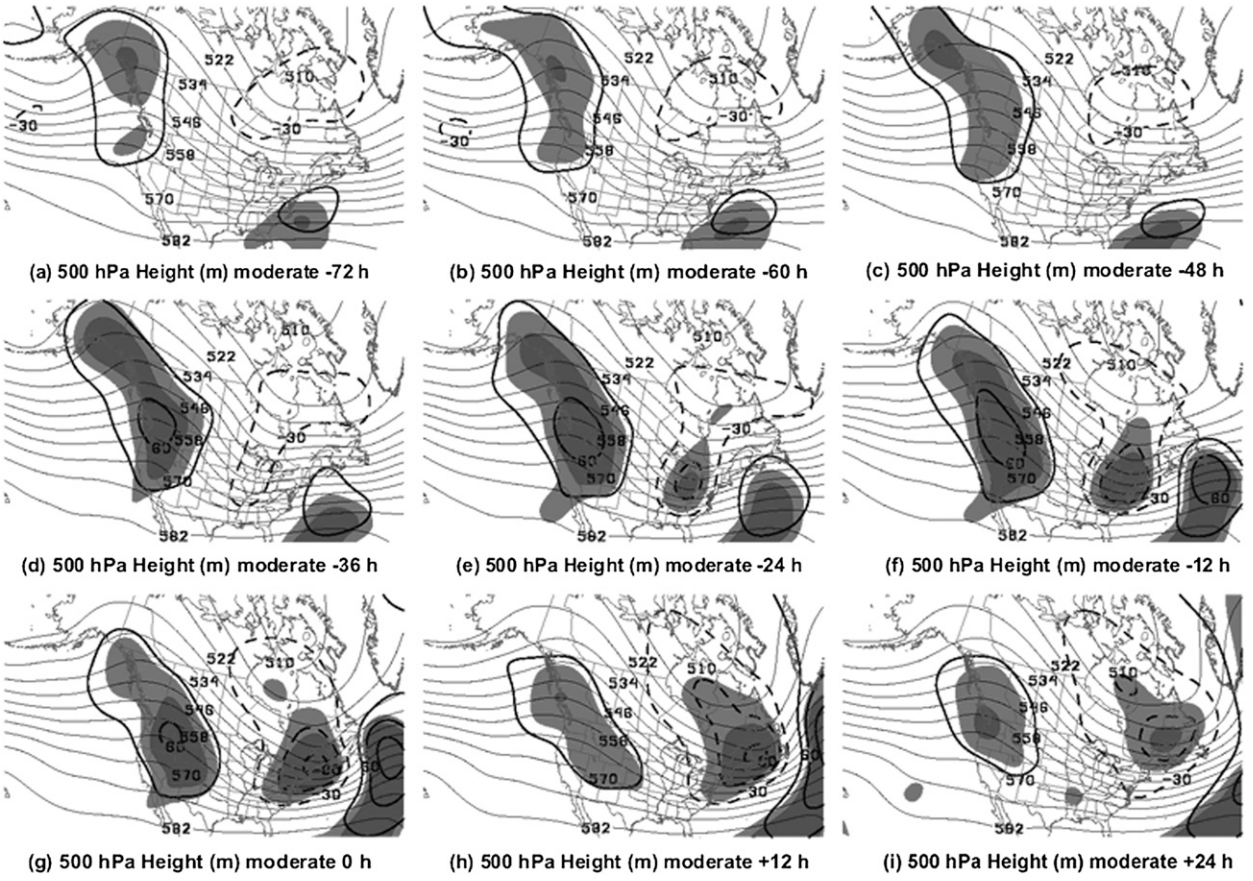

FIG. 9. As in Fig. 7, but for the moderate cases.

previously discussed (Fig. 11), starting at $t = -12$ h, near 70° and 40°W, respectively.

d. Precipitable water

Precipitable water composites are examined to explore the differences in terms of moisture among the various precipitation intensities, in addition to the basic synoptic structures examined in the SLP and 500-hPa height fields. The precipitable water field allows us to compare the moisture source location and amount associated with each precipitation intensity category.

1) EXTREME PRECIPITATION CASES

It was shown using the sea level pressure field that the cyclones responsible for the extreme precipitation cases at St. John's appear to originate near the Gulf of Mexico in the southeastern United States. Indeed, a statistically significant positive precipitable water anomaly appears over northern Florida at $t = -48$ h (Fig. 13a). This anomaly proceeds to rapidly intensify as it moves northeastward in the Atlantic Ocean toward St. John's, reaching a maximum intensity of 14 mm at $t = 0$ h (Fig. 13e) near St. John's. In addition, a significant negative precipitable water anomaly forms upstream of the positive anomaly, reaching a maximum intensity of −6 mm at $t = 0$ h (Fig. 13e) and creating a strong anomaly couplet.

2) MODERATE PRECIPITATION CASES

In the moderate cases, a statistically significant positive anomaly appears at 72 h prior to the event ($t = -72$ h; not shown), in contrast to 48 h prior to the event in the extreme cases. In addition, the positive anomaly in the moderate cases originates ($t = -48$ h; Fig. 14a) a bit farther to the north and west, in the eastern Ohio River valley. It was suggested earlier that the moderate composite contains the most variability among cyclone tracks; this theory is also supported by the large areal extent of the negative precipitable water anomaly behind the cyclone, which ranges from the Gulf Coast region of the United States to southern Quebec at $t = 0$ h (Fig. 14e). Finally, the elongated positive moisture anomaly in the Atlantic Ocean (Fig. 14e) is unique to the moderate cases (albeit a hint of such a feature can be seen in the extreme composite; Fig. 13). This feature suggests the possibility of a low-level jet or warm

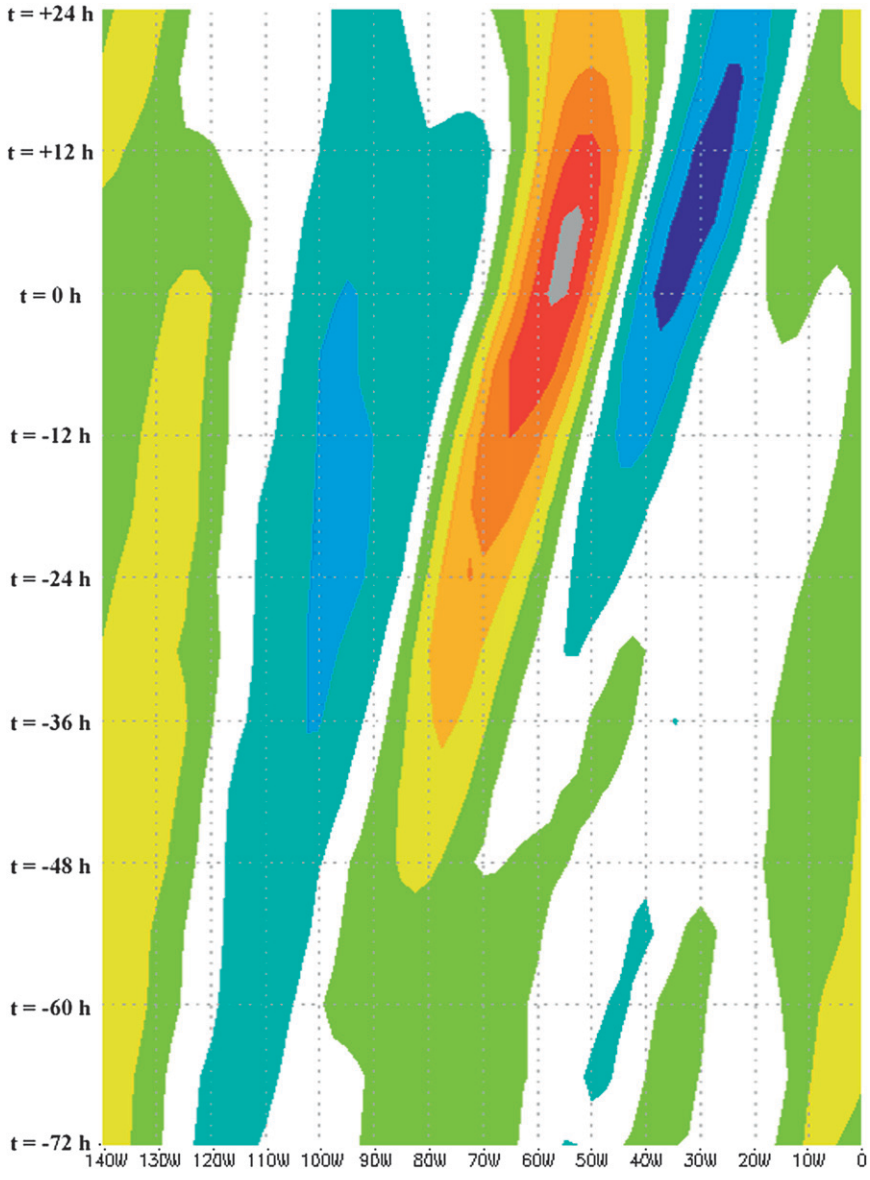

FIG. 10. As in Fig. 8, but at 45°N and for the moderate cases.

conveyor belt in advance of the cold front (i.e., the boundary between positive and negative precipitable water anomalies).

3) LIGHT PRECIPITATION CASES

As was the case in the SLP and 500-hPa height fields, the light precipitable water composite is structurally unique among the three precipitation intensities. First, a significant positive anomaly does not become apparent until 12 h before the maximum precipitation falls at St. John's ($t = -12$ h; Fig. 15d). It is not a coincidence that the appearance of this anomaly occurs just as the cyclone moves over water for the first time (Fig. 6d). This gives even more credence to the claim that the light cases are predominantly moisture-starved Alberta clipper systems that only become significant when they reach the first moisture source they encounter—the Atlantic Ocean. In terms of precipitable water, the positive anomaly only reaches a maximum (highest closed contour) of 6 mm at $t = 0$ h (Fig. 15e) near St. John's, and the anomaly couplet is much weaker (and has a much later time of onset) than in the other intensity composites. It is therefore clear from the precipitable water field that the moisture source region plays a large role in the eventual amount of precipitation received at St. John's, and that significant differences exist between the precipitation intensities, regardless of the variability within a particular intensity.

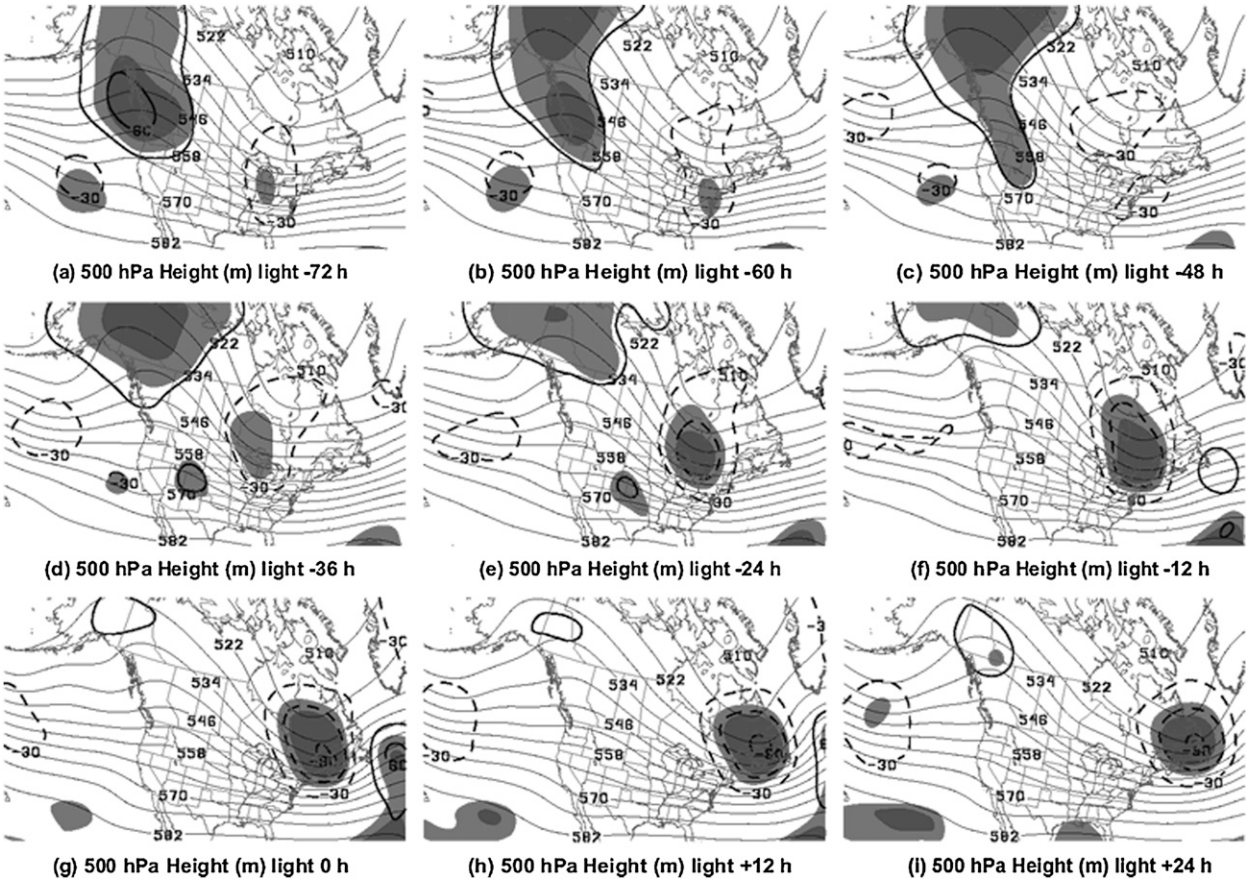

FIG. 11. As in Fig. 7, but for the light cases.

5. Wind analysis

a. Background and climatology

To complete the synoptic analysis of the three precipitation intensities, it is useful to examine the winds at the time of heaviest precipitation, $t = 0$ h. Wind roses are utilized for this purpose because they show the frequency of occurrence of winds in specified wind direction sectors and wind speed classes, according to the Lakes Environmental Web site (information available online at http://www.lakes-environmental.com). In recent studies, Nadeau (2007) and Knowland (2008) have used wind roses to illustrate both synoptic-scale and terrain-induced flows and their effects at locations such as Iqaluit, Nunavut; Norman Wells, Northwest Territories; Montreal, Quebec; and Burlington, Vermont. In this paper, the 925-hPa geostrophic wind and the 10-m observed wind are both displayed using wind roses to illustrate (a) the wind climatology at St. John's and (b) the particular flows during certain classes (i.e., intensities) of precipitation events at St. John's. All wind roses displayed in this section are divided into 16 wind direction sectors and seven wind speed classes, which are calm, 1–4, 4–7, 7–11, 11–17, 17–22, and >22 kt.

The wind climatology for the period of 1979–2005 at St. John's is displayed for both the 925-hPa geostrophic wind (Fig. 16a) and the 10-m observed wind (Fig. 16b). It is evident that the dominant geostrophic wind direction on a climatological basis at 925 hPa ranges anywhere from southwesterly to northwesterly, with pure westerly flow being the primary wind direction sector (Fig. 16a). While not a focus of this paper, terrain-induced channeling, friction, or both seem to skew the climatological distribution toward more southwesterly flow when looking at the 10-m wind, although pure westerly flow remains the primary sector (Fig. 16b). However, this difference is mitigated upon examination of the wind climatology in the cool season only (Fig. 17). From October to April, westerly flow is dominant in both the 925-hPa geostrophic wind (Fig. 17a) and the 10-m wind (Fig. 17b).

b. Wind roses during precipitation events

Wind roses are displayed for the 50 extreme precipitation cases described in detail in section 4 (Fig. 18).

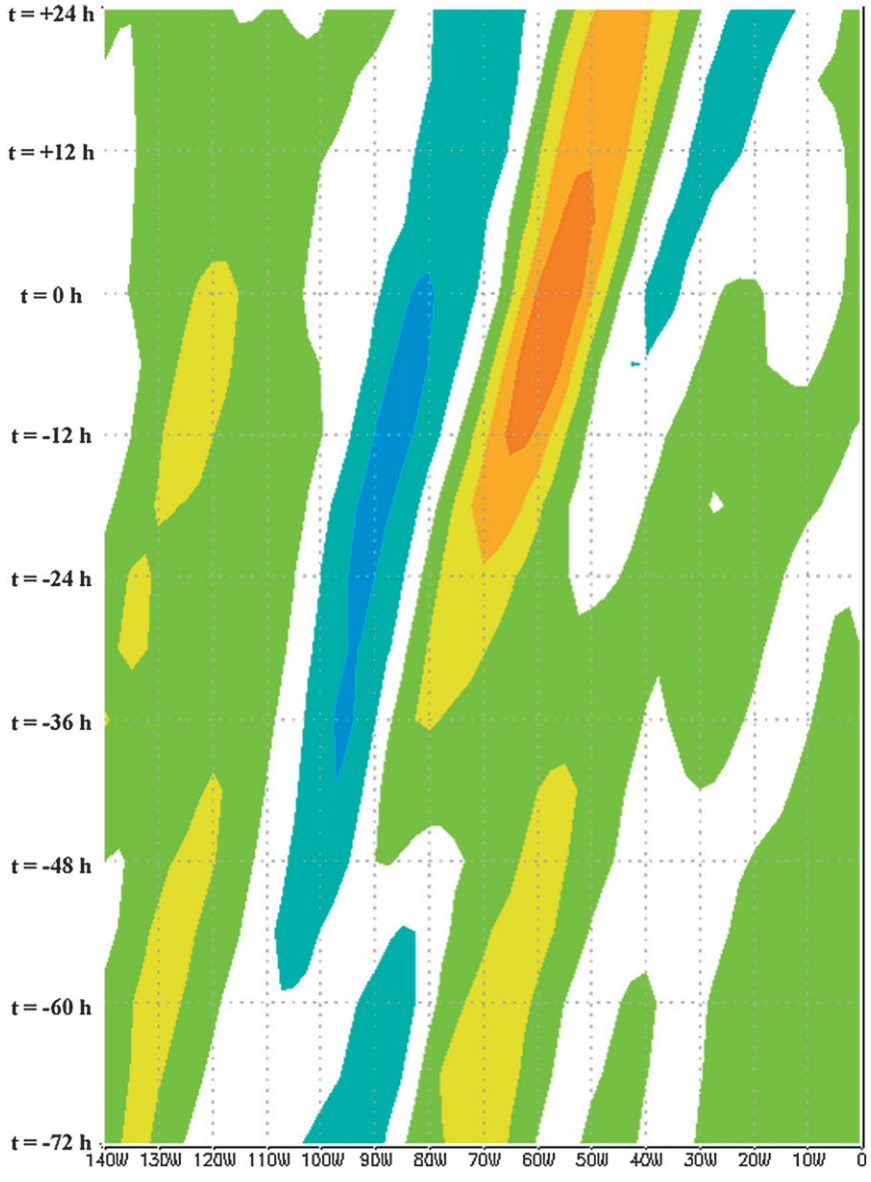

FIG. 12. As in Fig. 8, but at 45°N and for the light cases.

While the climatological wind direction at St. John's is from the west, it is evident that extreme precipitation events are associated winds that are predominantly out of the south-southeast (925-hPa geostrophic) and east (10 m) at $t = 0$ h (Fig. 18). The geostrophic wind (Fig. 18a) is representative of the sea level pressure pattern observed in the extreme composite (Fig. 5g); this pattern involves a strong maritime low pressure system located to the south-southwest of St. John's and moving northeasterly over time.

A clockwise rotation of the 925-hPa geostrophic wind distribution at $t = 0$ h from the extreme (Fig. 18a) to the moderate composite (Fig. 19a) is evident, with the predominant wind direction sector being south-southwesterly and a secondary maxima of southerly flow. This finding is consistent with a more continental-based storm track originating in the Ohio River valley as described in section 4b. It is interesting to note that the 10-m observed wind profile (Fig. 19b) for the moderate cases also shows a similar clockwise rotation, with the primary wind direction sector being south-southeasterly. However, a strong secondary sector is found at easterly flow, perhaps suggesting that, as mentioned earlier, the moderate cases contain the largest track variability of any precipitation intensity class.

The clockwise rotation of the 925-hPa geostrophic wind distribution (Fig. 20a) described above concludes in the light events composite, where while the predominant

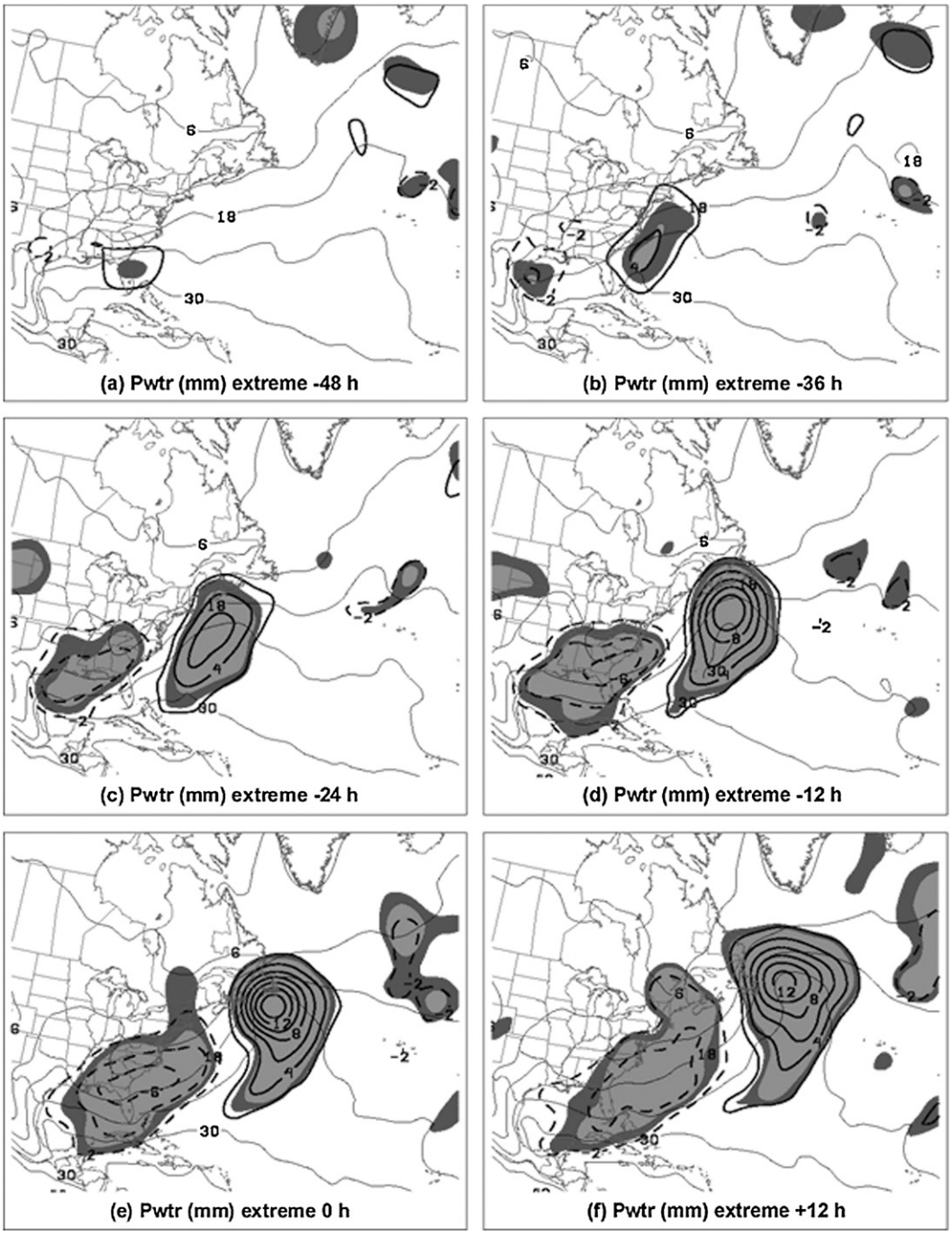

FIG. 13. Precipitable water anomalies every 2 mm, heavy dashed for negative values and heavy solid for positive values, with respect to climatology, for the extreme cases at (a) −48, (b) −36, (c) −24, (d) −12, (e) 0, and (f) +12 h. Light solid contours represent the full composite precipitable water field every 6 mm. Shading represents the statistical significance of the anomalies at the 95% (lighter shading) and 99% (darker shading) confidence levels, according to the Student's *t* test.

wind direction sector is south-southwesterly (as in the moderate composite), secondary maxima are found in the southwesterly and west-southwesterly sectors. This is entirely consistent with the finding in section 4b that the composite cyclone responsible for the light precipitation events is most likely an Alberta clipper system that approaches St. John's from the west or west-northwest (Fig. 6g). Finally, it is of note that for all

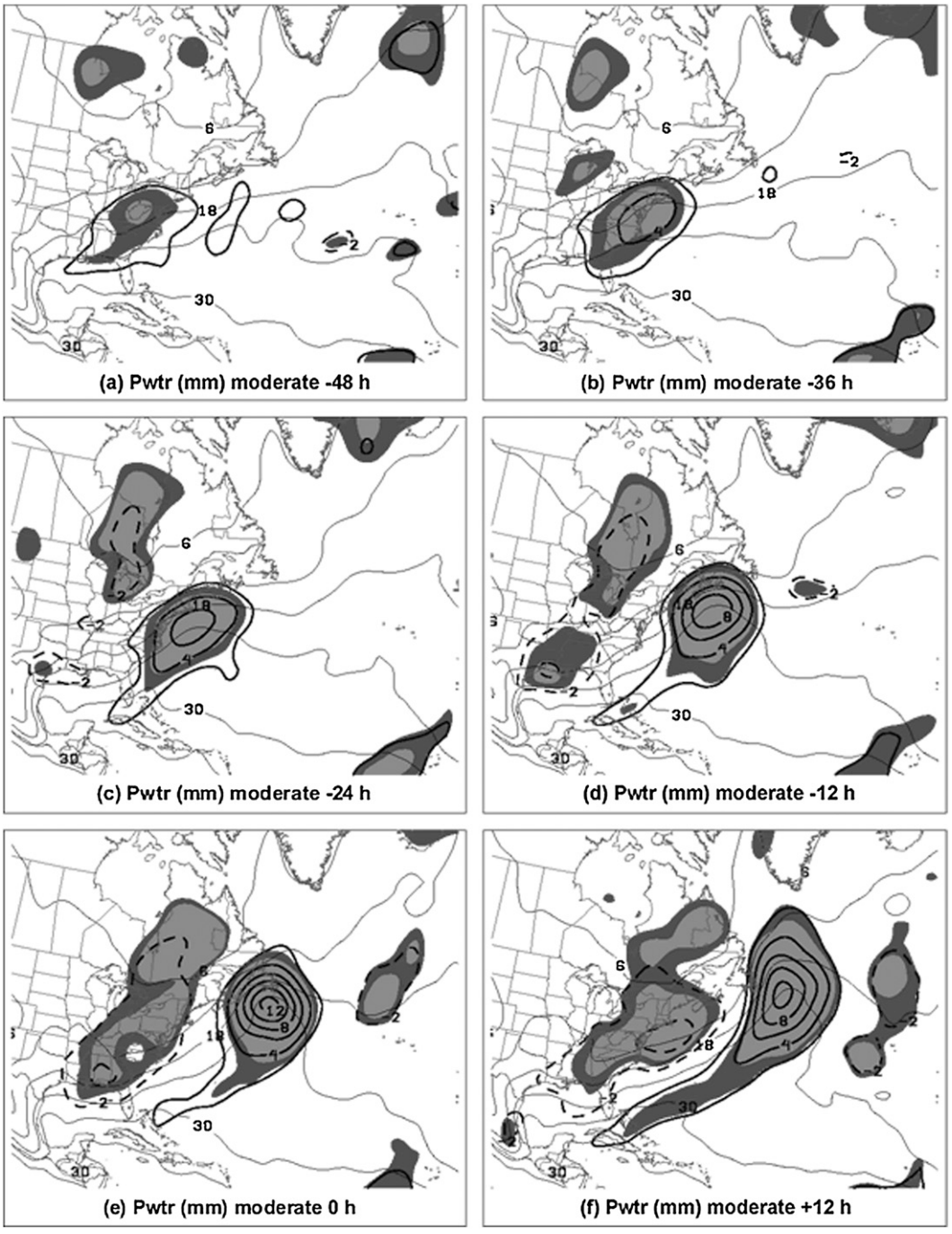

FIG. 14. As in Fig. 13, but for the moderate cases.

precipitation intensity categories, the 10-m observed wind distribution appears to be centered slightly counterclockwise of the 925-hPa geostrophic wind distribution. This difference can be explained primarily by friction, but again, it is possible that it is somewhat due to local terrain effects, a point that requires further investigation in the future.

6. Concluding discussion and future work

In this study, a precipitation climatology is assembled and statistically analyzed for St. John's, Newfoundland (CYYT), for the period of 1979–2005. During this time period, 1983 measurable (0.2 mm or greater) precipitation events lasting no more than 48 h are found to have affected St. John's. Events are then divided into three

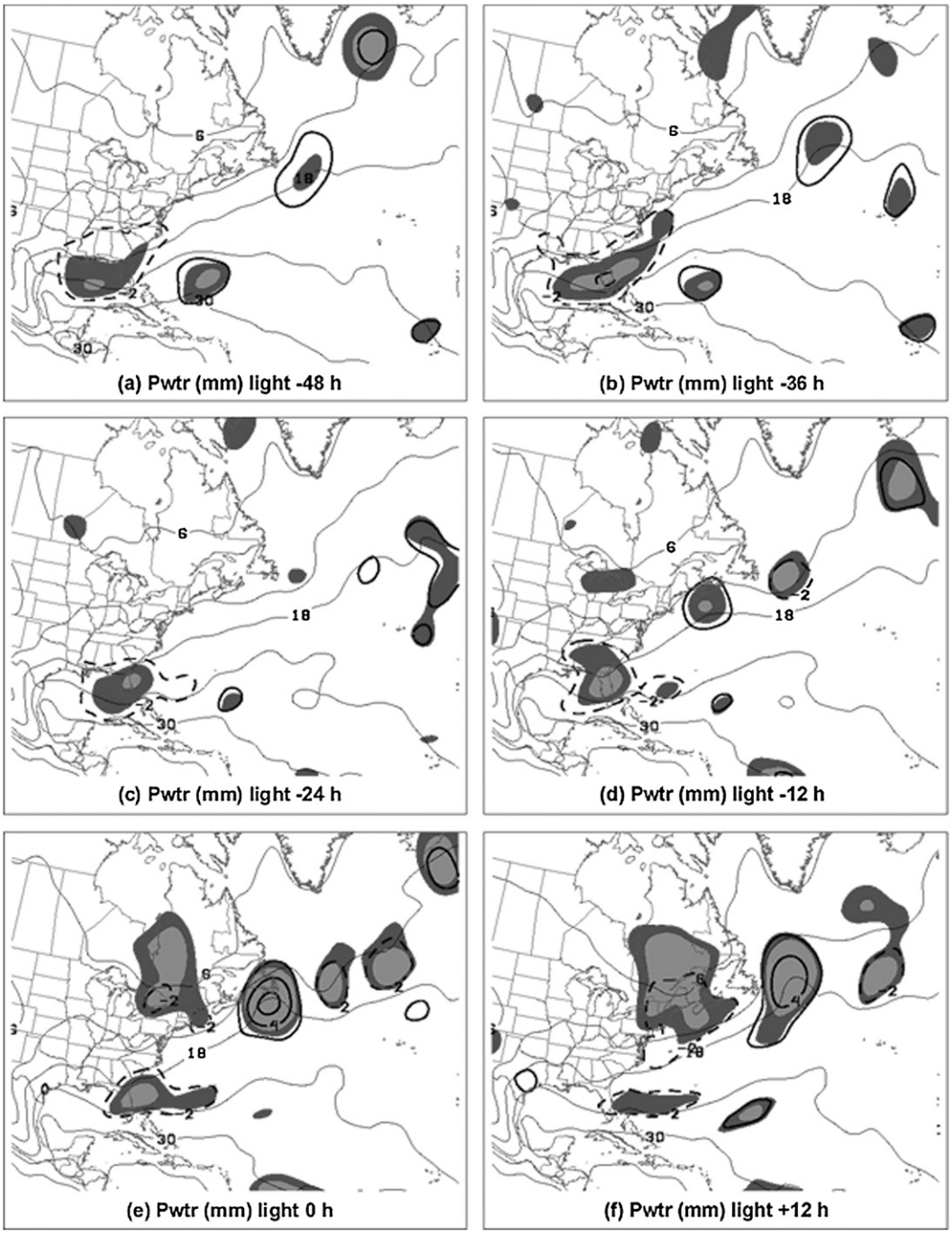

FIG. 15. As in Fig. 13, but for the light cases.

intensity categories (extreme, moderate, and light) based on the mean and standard deviation, as described in section 3. To evaluate the synoptic structures associated with each precipitation intensity category, 50 events are selected from each category. This is done by choosing the 25 events above and 25 events below the median precipitation amounts in each intensity category.

Once the 50 events from each precipitation category have been chosen, composite and anomaly plots (relative to a 1971–2000 monthly weighted climatology) from the NCEP–NCAR global reanalysis are completed in order to compare synoptic structures and precursors among the three precipitation intensity categories. In the SLP field for the extreme cases, a statistically

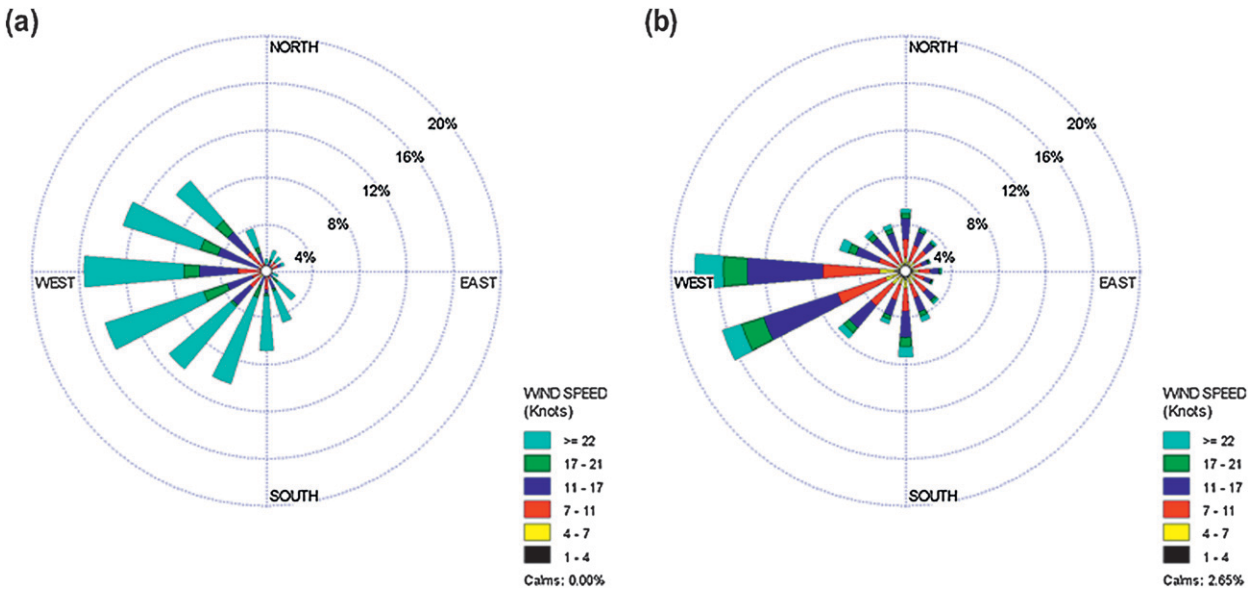

FIG. 16. Wind rose climatology for the period from 1979 to 2005, all months inclusive, at St. John's (CYYT) for (a) 925-hPa geostrophic and (b) 10-m observed winds, from station data. Wind classes are as follows: 1–4 (black), 4–7 (yellow), 7–11 (red), 11–17 (blue), 17–21 (green), and >22 kt (turquoise).

significant negative anomaly is depicted over the southeastern United States (Fig. 4), 2 days ($t = -48$ h) prior to the onset of heaviest precipitation at St. John's. This anomaly then tracks northeastward and reaches St. John's at $t = 0$ h, with a peak strength of −18 hPa. Precursor negative anomalies are also observed in moderate (Fig. 5) and light (Fig. 6) composites, but all of these anomalies differ in two respects: the initial time of observation and, more importantly, the initial region of observation. While the precursor negative anomaly in the extreme composite is centered near the Gulf Coast region over the southeastern United States, the precursor negative anomalies in the moderate (Ohio River valley region) and light cases (upper Midwest region of the United States) are initially observed significantly farther to the north and west of the anomalies in the

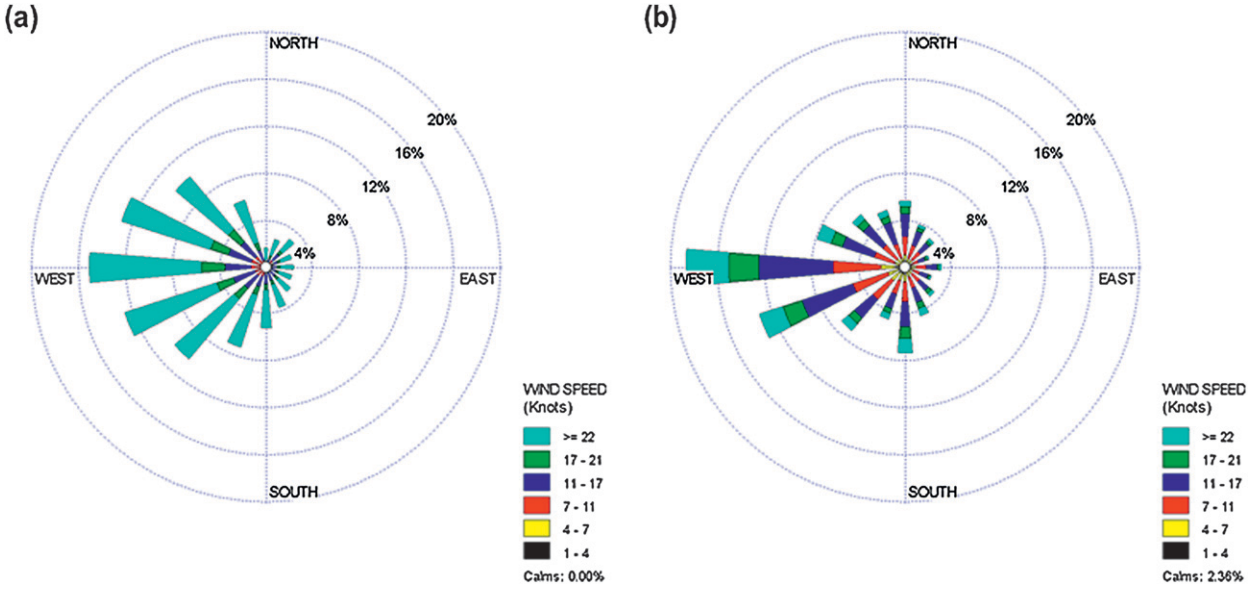

FIG. 17. As in Fig. 16, but for 1979–2005, October–April only.

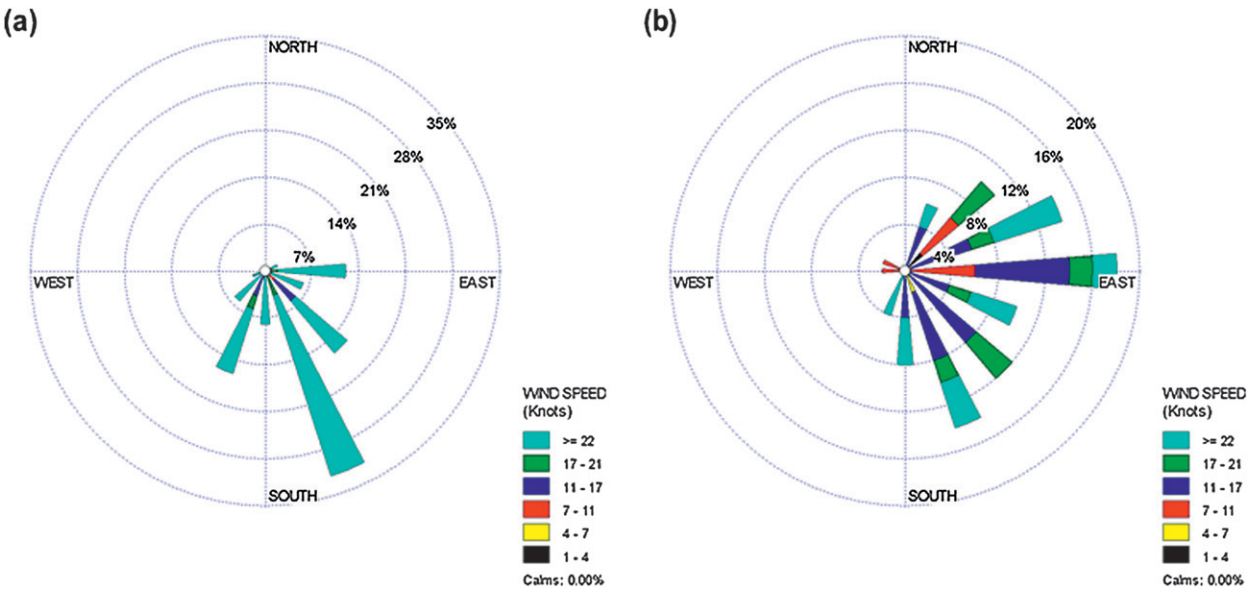

FIG. 18. As in Fig. 16, but for the 50 extreme precipitation cases only, at $t = 0$ h.

extreme composite. This observation leads to the conclusion that with decreasing precipitation amount, the track of the SLP anomaly becomes less meridional and more zonal. In other words, there is a clockwise rotation of both the initial observation area and composite storm track as the precipitation intensity category decreases from extreme to light. Additionally, the intensity of the downstream high pressure system is significantly greater in the extreme composite than it is in the moderate and light cases. This suggests that both the strength of the negative SLP anomaly (through low-level warm-air advection) and the intensity of precipitation (through latent heat release) act to strengthen the upper-level ridge and thus indirectly impact the intensity of the downstream positive SLP anomaly (as described in section 4b). Finally, it is of note that the average duration of the events (in 6-h precipitation periods) is considerably shorter in the light and moderate groups than in the extreme cases. Due to space considerations, these results are not graphically shown in the paper, although it has been concluded that of the 50 extreme events, only 6 lasted less than 24 h (or four precipitation periods), while there are 19 and 29 such events in the moderate and light cases, respectively. This suggests that duration, in addition to anomaly intensity, differs among the three composite groups, although duration and intensity are not necessarily independent of each other.

Composite anomaly plots of 500-hPa height depicted in section 4c are used to examine upper-level synoptic structures associated with each precipitation intensity category. The extreme (Fig. 7) composite demonstrates that a statistically significant precursor positive height anomaly is observed over the Pacific Northwest region of the United States at $t = -72$ h, or 3 days prior to the onset of heaviest precipitation observed at St. John's. This precursor anomaly dissipates over time concurrent with a significant negative anomaly and second positive anomaly building downstream. Additionally, the formation of downstream anomalies (Fig. 8) is at least in part due to Rossby wave propagation, as was also noted by Lackmann and Gyakum (1996). While the precursor positive anomaly in the moderate composite is located much farther to the north at $t = -72$ h over British Columbia, downstream Rossby wave propagation does appear to play a role in the formation of the downstream negative and positive anomalies (Fig. 10). The light case composite reveals that (a) there is no precursor anomaly at $t = -72$ h over the west coast (Fig. 11) and (b) downstream development due to Rossby wave propagation is weaker and has a later time of onset in our analysis (Fig. 12). There is also less southward impingement of the 500-hPa trough (negative anomaly) over the eastern United States, associated with the precipitation-causing cyclone, with decreasing precipitation amount. Finally, it is of note that a quick calculation (not shown here) of the Rossby wave phase speed both (a) agrees with the observed speed of translation of the primary trough in each composite and (b) that the primary trough in each composite is faster moving in the light as compared to the moderate cases and in the moderate cases as compared to the extreme composite. This supports the assertion mentioned above that duration

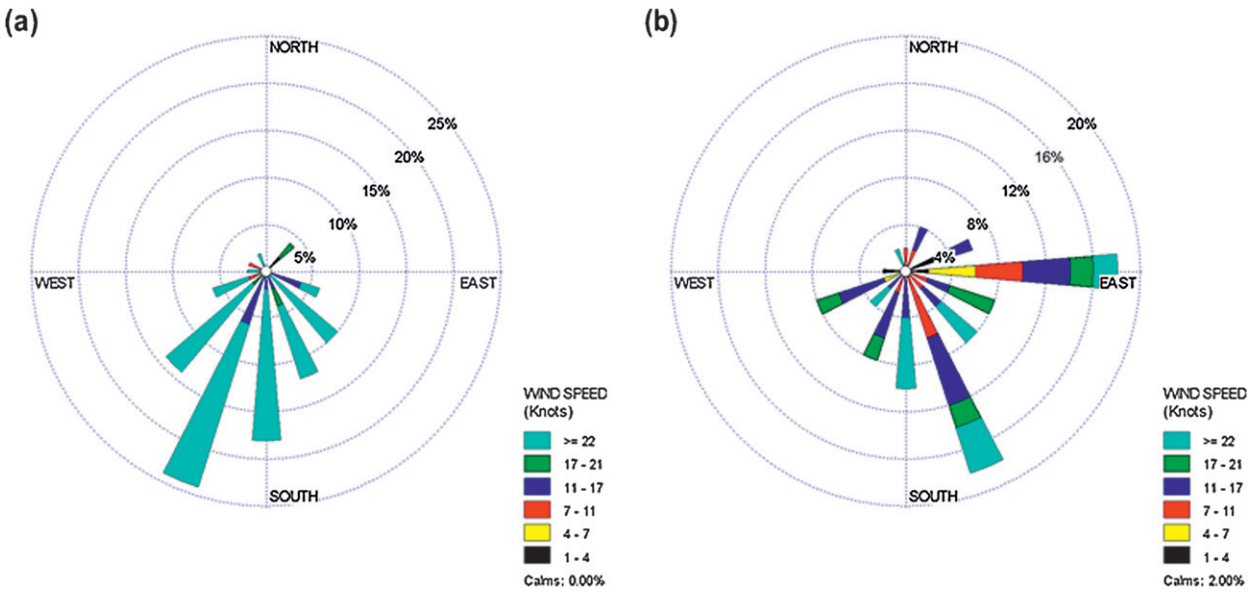

FIG. 19. As in Fig. 16, but for the 50 moderate precipitation cases only, at $t = 0$ h.

and intensity of the precipitation-causing features are both in play.

Precipitable water composite anomaly plots are presented in section 4, in order to evaluate the amount and origin of the moisture associated with each precipitation intensity category. From these analyses, several conclusions are drawn:

- In the extreme cases, a significant positive precipitable water anomaly can be seen as early as $t = -48$ h over northern Florida. The initial location of this positive anomaly travels progressively farther to the north and west with decreasing precipitation amount, signaling a more continental-based moisture source for the lesser-intensity categories. This is also consistent with the clockwise rotation of storm tracks seen in the SLP composites.
- The time at which a statistically significant positive precipitable water anomaly becomes visible is different for the various precipitation intensities. For example, in the extreme composite, an anomaly is first seen at $t = -48$ h; $t = -72$ h in the moderate; and

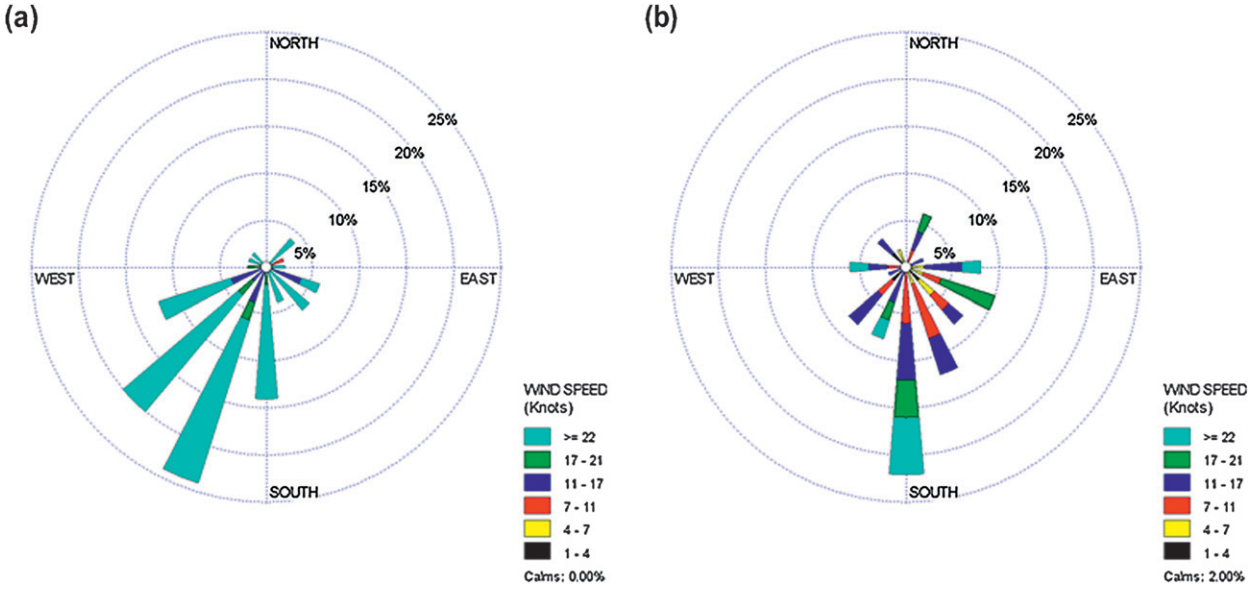

FIG. 20. As in Fig. 16, but for the 50 light precipitation cases only, at $t = 0$ h.

not until $t = -12$ h in the light composite. It is suggested here that this is at least partially a result of composite smearing.

- The results in the precipitable water analysis for the light cases are consistent with those shown in the SLP and 500-hPa height analyses. After completing a case-by-case map analysis, it is clear that the overwhelming majority of storm systems responsible for the light cases are Alberta clippers originating in the lee of the Canadian Rockies. In fact, this system appears to be so moisture starved that a positive precipitable water anomaly does not appear until $t = -12$ h, when the cyclone finally reaches its first moisture source, the Atlantic Ocean.
- The moisture anomaly couplet in the extreme cases is noticeably stronger in the extreme composite than in the moderate and, especially, the light composites. The fact that very moist air is closely located to very dry air suggests a strong baroclinic zone in the region between the positive and negative moisture anomalies. This, in turn, would be a very conducive environment for low-level cyclogenesis, a reflection of which is seen in the extreme SLP composite (Fig. 4).

Finally, an analysis of the distributions of wind speed and direction at the time of heaviest precipitation at St. John's ($t = 0$ h) is performed in section 5. It is found that there is a preference for low-level (925 hPa) easterly and southeasterly geostrophic winds during extreme precipitation events at St. John's (Fig. 18). This direction is not favored at all in the cool-season climatology (Fig. 17). In addition, a clockwise rotation of the preferred 925-hPa geostrophic wind direction from east-southeasterly to southwesterly occurs with decreasing precipitation amount. This observation is consistent with both the SLP and precipitable water fields, where a clockwise rotation of the composite storm track is observed. In other words, a more meridional, ocean-based storm track in the extreme cases is more likely to produce an easterly geostrophic wind at St. John's, whereas a more zonal, continental-based storm track in the light cases is more apt to produce a southwesterly geostophic wind, with the moderate composite somewhere in between. Additionally, the more easterly near-surface winds seen in the extreme composite implies more veering (and thus warm-air advection) throughout the column, compared with the moderate and light cases. This, combined with the finding of the stronger baroclinic zone in the extreme composite described above and the longer average duration of extreme events, suggests that the extreme composite shows more forcing for ascent over a generally longer period of time (and thus, presumably, more precipitation) than the lesser composites, and should be viewed as a signal that a forecaster would be able to look for during and before extreme events.

There is much work to be done in the analysis of significant precipitation events at St. John's. Future work will include but not be limited to an investigation of the variability of storm tracks and synoptic structures *within* each precipitation category; an examination of radar images for a subset of precipitation events, to assess the importance of precipitation banding; and an evaluation of precipitation events with regard to the North Atlantic Oscillation (NAO). The authors hope that answers to these questions will provide insight and knowledge to the local forecaster, which will help to improve short-term forecasts at St. John's and similar stations.

Acknowledgments. This research has been supported by grants from the Natural Sciences and Engineering Research Council of Canada and the Canadian Foundation for Climate and Atmospheric Sciences. Special thanks to the National Centers for Environmental Prediction (NCEP) for providing access to the NCEP Global Reanalysis and the North American Regional Reanalysis. Finally, thanks to Gerard Morin at the Atlantic Climate Centre of Environment Canada for providing access to the 6-hourly precipitation data.

REFERENCES

Atallah, E. H., J. R. Gyakum, P. A. Sisson, M. Kimball, and A. Roberge, 2005: Warm season extreme quantitative precipitation forecasting for the Burlington, VT region. Preprints, *21st Conf. on Weather Analysis and Forecasting/17th Conf. on Numerical Weather Prediction*, Washington, DC, Amer. Meteor. Soc., P1.20. [Available online at http://ams.confex.com/ams/pdfpapers/94807.pdf.]

Bosart, L. F., 1981: The Presidents' Day snowstorm of 18–19 February 1979: A subsynoptic-scale event. *Mon. Wea. Rev.,* **109,** 1542–1566.

Doswell, C. A., III, H. E. Brooks, and R. A. Maddox, 1996: Flash flood forecasting: An ingredients-based methodology. *Wea. Forecasting,* **11,** 560–581.

Fischer, A. P., 1997: A synoptic climatology of Montreal precipitation. M.S. thesis, Dept. of Atmospheric and Oceanic Sciences, McGill University, 71 pp.

Hart, R., and J. Evans, 2001: A climatology of the extratropical transition of Atlantic tropical cyclones. *J. Climate,* **14,** 547–564.

Kalnay, E., and Coauthors, 1996: The NCEP/NCAR 40-Year Reanalysis Project. *Bull. Amer. Meteor. Soc.,* **77,** 437–471.

Knowland, K. E., 2008: A study of the meteorological conditions associated with anomalously early and anomalously late openings of a Northwest Territories winter road. M.S. thesis, Dept. of Atmospheric and Oceanic Sciences, McGill University, 72 pp.

Koch, S., M. DesJardins, and P. Kocin, 1983: An interactive Barnes objective map analysis scheme for use with satellite and conventional data. *J. Climate Appl. Meteor.,* **22,** 1487–1503.

Lackmann, G. M., and J. R. Gyakum, 1996: The synoptic and planetary-scale signatures over the Mackenzie River basin. *Atmos.–Ocean,* **34,** 647–674.

——, and ——, 1999: Heavy cold-season precipitation in the northwestern United States: Synoptic climatology and an analysis of the flood of 17–18 January 1986. *Wea. Forecasting,* **14,** 687–700.

Mekis, E., and W. D. Hogg, 1999: Rehabilitation and analysis of Canadian daily precipitation time series. *Atmos.–Ocean,* **37,** 53–85.

Nadeau, D., 2007: Impacts of synoptic atmospheric circulations and topographic conditions on sustained strong surface winds over southern Nunavut. M.S. thesis, Dept. of Atmospheric and Oceanic Sciences, McGill University, 129 pp.

Roebber, P. J., and L. F. Bosart, 1998: The sensitivity of precipitation to circulation details. Part I: An analysis of regional analogs. *Mon. Wea. Rev.,* **126,** 437–455.

Sisson, P. A., and J. R. Gyakum, 2004: Synoptic-scale precursors to significant cold-season precipitation events in Burlington, Vermont. *Wea. Forecasting,* **19,** 841–854.

Stewart, R. E., R. W. Shaw, and G. A. Isaac, 1987: Canadian Atlantic Storms Program: The meteorological field project. *Bull. Amer. Meteor. Soc.,* **68,** 338–345.